Open Ceramics 20 (2024) 100704

Contents lists available at ScienceDirect

Open Ceramics

journal homepage: www.sciencedirect.com/journal/open-ceramics

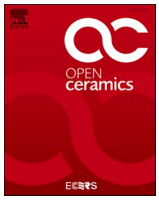

Effect of water-to-quick setting cement ratio and aggregate size on mechanical properties and dimensional accuracy of binder jetting 3D-printed bodies

Mursaleen Shahid *, Vincenzo M. Sglavo

Department of Industrial Engineering, University of Trento, Italy

ARTICLE INFO

Keywords:
Binder jetting 3D printing
Quick setting cement
Water-cement ratio
Aggregate size
Strength
Printing accuracy

ABSTRACT

Quick setting cement-based materials were produced in the present work using the binder jetting 3D printing (BJ3DP) technique with the aim at investigating how processing parameters like water-to-cement ratio and aggregate size affect the final properties of the products. Commercially available quick-setting cement and siliceous sand were utilized. Dimensional accuracy, compressive and flexural strength were measured for variable processing conditions and their individual effect was analysed. The results showed that the properties of printed parts are significantly influenced by the considered processing variables and, in particular, a larger water-to-cement ratio has a beneficial effect on the mechanical performances, the improvement being higher when coarser siliceous sand is used. It was also shown that the employment of finer sand results in more limited dimensional accuracy.

1. Introduction

The processing of cement-based materials using additive manufacturing (AM) has attracted a lot of attention from the building industry [1,2]. This shift opens a new world of possibilities, as additive manufacturing techniques promise to streamline construction processes and overcome the limitations of traditional methods. In recent years, robocasting and binder jetting 3D printing (BJ3DP) have shown themselves to be competitive substitutes for the production of cement-based materials [3,4]. Robocasting is an extrusion-based additive manufacturing technique where the concrete paste is extruded using a gantry, crane or robotic arm mechanism [5–7]. BJ3DP technique includes the layering of powder or aggregate and selective deposition of a liquid binder [8] to consolidate the desired shape layer by layer [9–12]. After hardening, the unbonded powder is methodically removed, paving the way for separate post-processing techniques aiming at achieving the desired levels of strength and durability [13–17]. An early investigation of this method was carried out by Zhou et al. [18]., who studied the use of calcium sulphate hemihydrate (CaSO4.0·5H2O) in 3D printing. The potential of binder jetting technology to create high-quality parts at a lower cost and faster rate compared to conventional manufacturing procedures has attracted a lot of interest in recent years [19].

Cement-based materials have been used in BJ3DP because of their unique properties such as high compressive strength, durability and fire resistance [20,21]. They are mainly composed of cement, aggregates and water, although their properties can be enhanced by using additives such as plasticizers, retarders and accelerators [22]. The use of cement-based materials through the BJ3DP technology offers many advantages such as increased design freedom, reduced material waste and improved sustainability [23]. Additionally, the technology makes it possible to create intricate shapes and structures that would be challenging to obtain with traditional manufacturing methods. However, this integration has forced the creation of unique mix-design protocols that are tailored to the requirements of 3D printing. It is important to remember that not all material compositions work well with the complex nature of 3D printing. Researchers have conducted significant investigations on various types [22,24–27] and amounts of cement and sand combinations [12,27–30], mostly utilizing commercially available ordinary Portland cement with sand [31]. In a previous study by Pegna [32], the use of ordinary Portland cement combined with a silica sand layer was studied for the 3D printing of mortar components. In earlier researches, specific compositions and methods used for mixing, especially with reference to the water-to-cement ratio, have not been thoroughly explained.

* Corresponding author.
E-mail address: Mursaleen.Shahid@unitn.it (M. Shahid).

https://doi.org/10.1016/j.oceram.2024.100704
Received 20 June 2024; Received in revised form 7 November 2024; Accepted 11 November 2024
Available online 13 November 2024

BJ3DP of cement-based materials is primarily influenced by the inert powder size, morphology and binder content. Several studies have been carried out and have investigated the effect of such printing parameters [14,22,33,34]. Among the variables, the characteristics of the binder flow are essential for getting the desired printing results. Xia et al. [35] analysed the effects of binder saturation level on dimensional accuracy and compressive strength. In such work, the effects of various printing parameters, such as shell-to-core ratio and binder saturation level on the dimensional correctness and compressive strength of the specimens were examined. The findings show that changing the shell/core ratio from 1:1 to 1:2 and increasing the binder saturation level significantly boosts the compressive strength. Lowke et al. [33,36] also explored the effect of the binder content using an aqueous solution on a fine cement-aggregate composite with particles smaller than 0.45 mm while employing the selective cement activation technique. Methylcellulose thickening agent was also considered in the composition to improve the printing accuracy. An increase of compressive and flexural strength was observed to be due to wider water distribution within the layers. The study of McEleney et al. [37]also investigated the binder spreading behaviour onto the powder and the powder-binder wettability. They concluded that drop penetration increases with a reduction in macro-voids on the powder beds.

It is significant to note that spherical and coarse powders show variation in spread among adjacent particles [38]. The flowability of the powder, which must be considered and maintained uniformly throughout the process, is another important parameter. Powders with higher flowability improve the resolution of the printed specimen and the powder with lower flowability has the worst impact on the resolution of the printed specimen [39]. The angle of repose, the Hausner ratio, the flow via an orifice, the Carr's compressibility index, the Shear cell method and the Cohesion index are the most used approaches to quantify the flowability of powders[40–43].

In the exploration of aggregate size's impact, Ling et al. [44] performed an insightful study on the influence of varying sand sizes on the mechanical performance of cement-based composites enhanced with polyvinyl alcohol fibre (PVA) and nano-SiO2 (NS). They concluded that finer sand sizes lead to reduced workability and mechanical strength. However, this effect was limited to sand particles below 380 μm.

In the context of BJ3DP, the selection of aggregates must be correlated with the flowability and thickness of the printed layers [45]. In a noteworthy work, Fan et al. [46] processed carbon powder particles with diameters up to 105 μm. Their method entailed using a furfuryl resin with an acetone base as a binder. The analysis showed that the printed structures' mechanical characteristics, before the sintering stage, reached a maximum value of 5 MPa. Chun et al. [47] found that larger silica sand grain sizes improved the penetration resolution and green body strength, particularly for 70 μm particle-sized sand. Pierre et al. [34] highlighted that to achieve optimal cohesion and high compressive strength, complete filling of the sand layer's thickness with cement paste was required. Pu et al. [48]used Burger`s model to simulate the rheological properties of OPC (Ordinary Portland Cement) paste and they discovered that yield stress is a function of particle size. For cement-based materials, significant consideration must be paid to aspects like powder size to get the appropriate printing results. Joseph et al. [43] examined a dry cementitious mix consisting of round-grain fine aggregates and calcium sulfoaluminate (CSA) cement. The results indicate that the addition of fine aggregates to CSA cement allowed the objects with rapid production capability and compatibility with conventional construction materials. Zhou et al. [47] focused on the surface homogeneity and roughness of both coarse and fine powders. They discovered that fine powder has a higher level of roughness and coarse powder has a higher level of surface uniformity.

In spite of the numerous works on BJ3DP applied to cement-based materials, a gap remains in exploring the influence of water-cement ratios on coarse and fine aggregate size and their significant impact on the mechanical properties and dimensional accuracy of 3D-printed concrete structures without additional viscosity modifying agents or thickening agents [36]. In addition, the use of materials such as quick-setting cement in the context of 3D printing, which could allow faster production systems, has not been extensively investigated.

The present study aims therefore at investigating the effects of the water-cement ratio considering two different aggregate sizes on the mechanical properties and dimensional accuracy of 3D-printed specimens using quick-setting cement.

1.1. Experimental procedure

A customized 3D printer was used in the present work where a single nozzle by Lee Co, USA was employed to spread the binder in drop on demand manner with the help of a Staiger valve. The process starts with the creation of CAD geometry using 3D modelling software and then slicing the model into a G-code to make it readable for 3D printing [49]. The layer thickness and distance between the printing head and the powder bed were kept at 2 mm and 10 mm, respectively [31]. Binder flow and water-to-cement ratio (w/c) were controlled by varying the travel speed of the printhead between 7200 mm/min and 13,000 mm/min and altering the water pressure in the 0.1 – 0.8 bar range [36].

Two different grain sizes of quartzite sand, namely 0.1 – 0.4 mm and 0.4 – 1.2 mm, were meticulously chosen for producing two different mixtures, called Mix-I and Mix-II. For the former, the finest sand was homogeneously mixed with commercially available quick-setting cement from Vicat in a proportion of 1:3 by weight. The 0.43 – 1.18 mm sand was combined with the quick-setting cement in the same weight ratio to produce the second one. The particle size distribution is shown in Fig. 1.

The quick-setting cement used in this study contains primarily a mixture of tricalcium silicate, dicalcium silicate, tricalcium aluminate and calcium ferroaluminate obtained by firing argillaceous limestone at 1000–1200 °C, along with calcite, spurrite, and minor proportions of lime, magnesia, sodium sulphate and potassium, with traces of other elements.

Both Mix-I and Mix-II were thoroughly and separately blended for 30 min to ensure the homogeneity of the powder mixture.

The blended powders' flowability was determined using the Hausner ratio and Carr's index [12]. These parameters were calculated according to the tap volume Vt and the loose bulk volume Vb of the powder as:

$$\text{Hausner ratio} = \frac{Vb}{Vt} \tag{1}$$

$$\text{Carr's Index} = \frac{(Vb - Vt)}{Vb} \text{x}100 \tag{2}$$

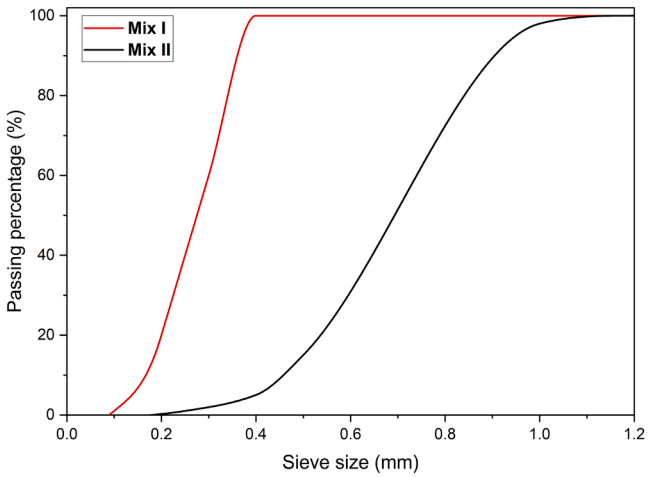

Fig. 1. Particle size distribution of the aggregates used in the present work.

A graduated cylinder, as per norm ASTM D7481–18, was used to measure the loose bulk volume of the mixtures. A tap density tester was used to determine the tap volume according to the same norm [50].

A schematic of the 3D printing process is shown in Fig. 2: the dry powder mixture is spread from the hopper bin over the build platform and then quickly flattened with a wiper blade. Using a single nozzle with an internal diameter of 0.19 mm, deionized water [12] was sprayed onto the powder bed from a pressurized vessel. Prismatic CAD models with dimensions 160 mm x 40 mm x 40 mm were printed as per norm EN 196–1[51] to measure the flexural strength; 40 mm edge cubes were printed for compressive strength testing (Fig. 2). After printing, the specimens were left in the powder bed for one day to undergo controlled curing. They were then removed from the powder bed and the excess powder was removed from the surface of the printed specimens by de-powdering: a fine bristled brush was used to manually remove the loose material from the surface of the samples and partially filled cavities on the outer geometry. This gentle manual removal of excess powder needs extra care as excess force might damage the printed layers.

The precision of the printed specimens establishes the level of conformity between the printed and the design dimensions. Vernier caliper was used to measure the dimensions of the printed specimens. Based on these measurements, the dimensional deviation ratio (DDR) and the X and Y printing precision in terms of xy-axis print precision were calculated to make assessments of printing accuracy [28,40]. By comparing the measured dimensions of the 3D-printed specimens to the CAD dimensions, the dimensional deviation ratio (DDR) was determined as:

$$DDR\ (\%) = \frac{L_P - L_{CAD}}{L_{CAD}} \times 100 \tag{3}$$

where L_p and L_{CAD} are the printed and initial dimensions defined in the CAD model of the specimen, respectively. The proportional variation between the measured dimensional values of the 3D-printed specimens and the desired dimensions was obtained also in terms of XY-axis printing precision:

$$XY - axis\ printing\ precision\ (\%) = \frac{A_p - A_o}{A_o} \times 100 \tag{4}$$

where A_p and A_o are the real printed area after de-powdering and the area of the 3D CAD file, respectively. Thirty measurements across the final layer were carried out to estimate accuracy. In contrast, the dimensional deviation ratio defines the linear discrepancies between dimensions in print and the nominal dimensions. Though complex geometries may not be captured with high precision by caliper, careful measurement at several touchpoints was done to reduce inaccuracy.

During post-processing, 80-grit sandpaper was used to refine the specimen into the required dimensions for mechanical testing. The specimens were set to be cured in air and were placed under a controlled hood for periods ranging from 1 to 28 days until mechanical testing was carried out.

An Anton Paar pycnometer (Ultrapyc 5000 series) was used to measure the true density of the printed samples after 7 days. Apparent and bulk density were determined as per the norm ASTM C-642 [52]and ASTM C-20 for porosity.

Mechanical tests were carried out on a universal mechanical testing machine (model 810, MTS Systems, Minneapolis, MN, USA) to determine flexural and compressive strength. The former was measured by a three-point bending test as:

$$\sigma_f = \frac{3Fl}{2bd^2} \tag{5}$$

where F, l, b and d are the maximum load, length, width and thickness of the specimen, respectively. A constant loading rate (50 ± 10 N/s) was used for the test.

For the compression test, the loading rate was kept at 2400 N/s and the strength σ_c was determined as the maximum load applied over the nominal cross-section of the sample (40 mm x 40 mm). Fig. 3

2. Results and discussions

The flowability data reveal interesting details about the two mixtures behaviour. The excellent flow characteristics of both Mix-I and Mix-II are demonstrated by their Hausner ratio equal to 0.86 and 0.9, respectively. Furthermore, their Carr's index is equal to 15.5 for Mix-I and 11.1 for Mix-II confirming that they are appropriate for the experiment. Notably, Mix-I shows somewhat better flow properties than Mix-II, thus highlighting its potential benefit in particular applications needing ideal flowability [18].

Fig. 4 shows the measured true, bulk, apparent density and porosity of 3D printed specimens. The results show that the density slightly increases moving from Mix-I to Mix-II. This can be very likely correlated to the different sizes of the sand used in the two mixtures which makes the

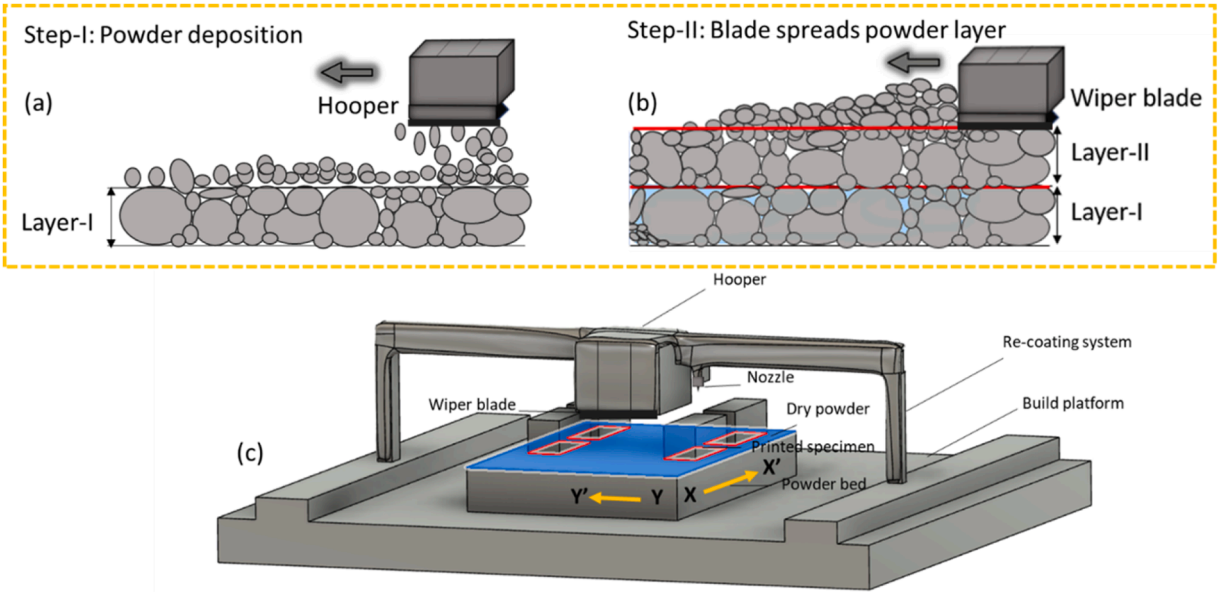

Fig. 2. (a, b) Powder deposition and spreading (c) Schematic of customized 3D printer.

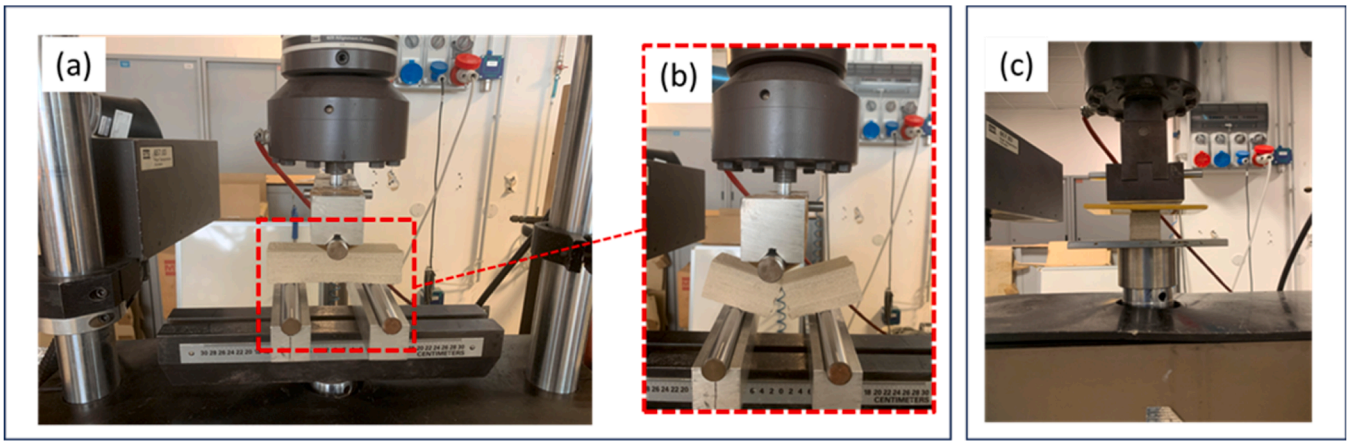

Fig. 3. (a) Flexural strength testing setup; (b) Fractured specimen after 3-point bending testing; (c) Compressive strength testing setup.

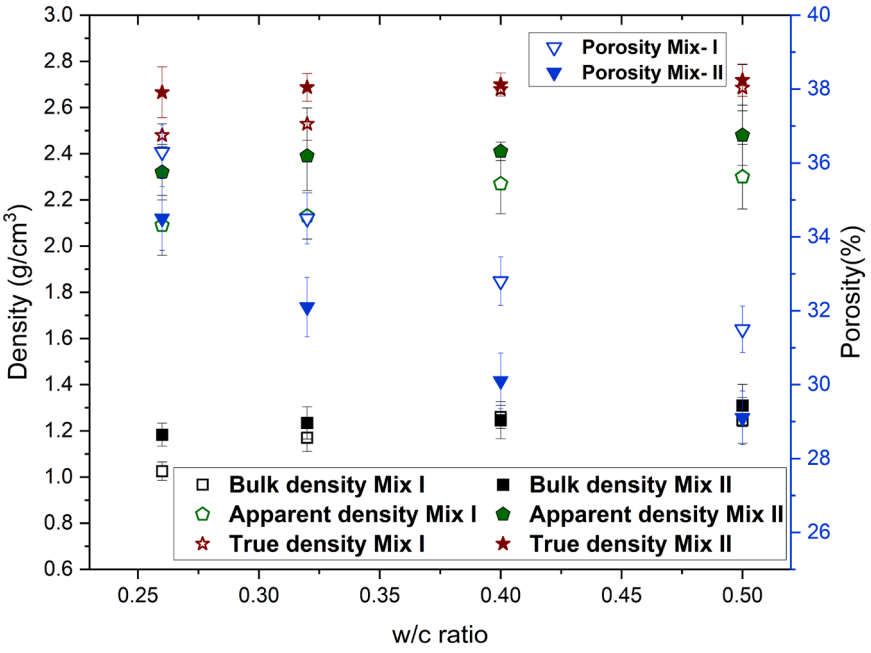

Fig. 4. Density and porosity of 3D printed samples for variable w/c ratio.

material produced with the coarser one more compact. The increased density observed in Mix-II might be mainly ascribed to the presence of coarser aggregate sizes in comparison to Mix-I. The interplay of particle size, shape, and packing properties has a considerable impact on overall density. The larger sand particles in Mix-II most likely increased inter-particle interactions and reduced particle segregation during a step of powder deposition and spreading, resulting in a denser concrete matrix. The effect of the water-to-cement ratio on density is very limited, the values being just slightly higher at larger w/c. In this case, the presence of more water allows more intense hardening reactions for the cement among the siliceous sand particles thus contributing to a more compact structure. By increasing the w/c ratio, the true density of 3D-printed parts increases as well. This may be attributed to the fact that at higher w/c ratios hydration increases and this could eventually lead to a denser microstructure in printed parts. Similar findings have been reported in the literature [53] where higher true density at increased w/c ratio was attributed to the potential of natural carbonation.

The flexural strength at various water-to-cement ratios and after different curing times is shown in Fig. 5. The strength of some samples after one day of curing was too weak and was not reported here. Notably, the relationship between flexural strength and water-to-cement ratio is substantially positive.

The effect can be related to the larger amount of water that penetrates between the layers and the sand particles with a beneficial effect on the cement hardening which strengthens the concrete structure, in agreement with previous results [54]. Correspondingly, as the curing time increases, the reactions can evolve thus making the bonding among the aggregate stronger. As the curing time increases, also the compressive strength of specimens cured in the air increases, as shown in Fig. 6. The steady rise in compressive strength over time is again indicative of the hydration process occurring in the cementitious materials which therefore become stronger. The conventionally produced concrete specimens were prepared using the same material composition as the 3D-printed specimens but with a water-cement ratio of 0.5. All conventionally produced specimens were cast by pouring the produced mortar into moulds and curing them under ambient conditions. The compressive strength measured for conventionally produced concrete specimens was 9.3 ± 2 MPa after 7 days of curing. Conversely, in the case of the 3D-printed specimen, the compressive strength with a water/cement ratio of 0.5 after 7 days was about 2.5 MPa. This

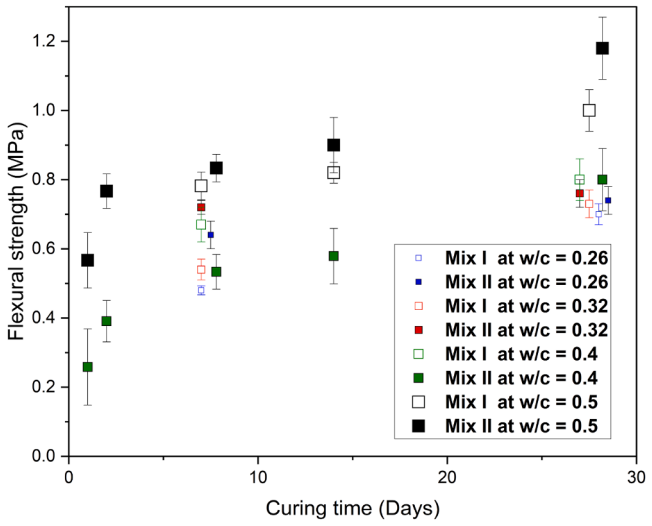

Fig. 5. Effect of water-cement ratio on flexural strength at different curing time.

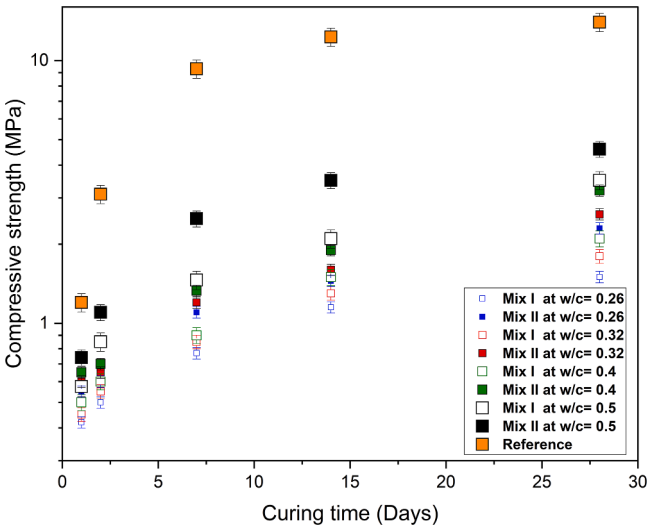

Fig. 6. Effect of curing time on compressive strength of Mix – I and Mix-II at different w/c ratio.

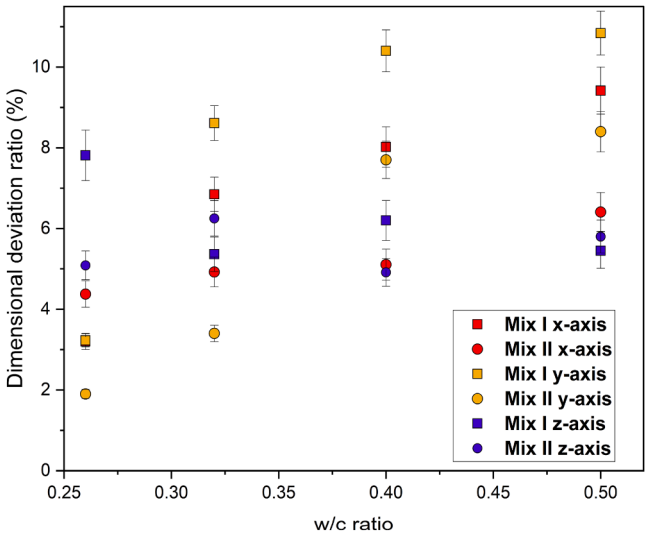

Fig. 7. Dimensional deviation ratio for different water-to-cement ratio.

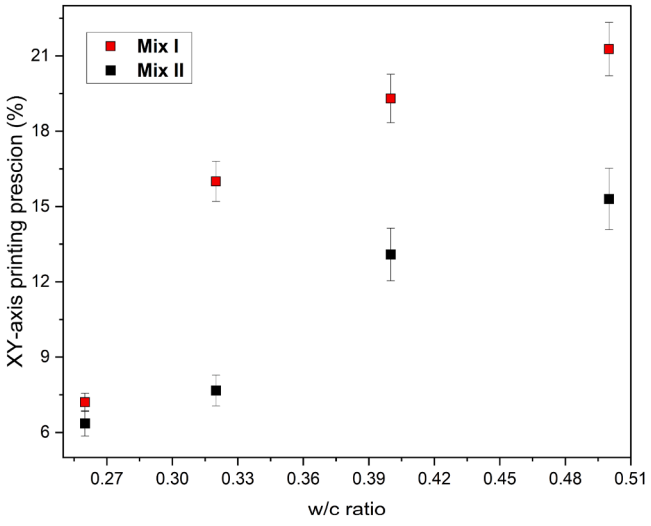

Fig. 8. XY-axis printing precision as a function of w/c ratio.

significant gap can be attributed to the fact that traditional casting methods allow denser structures with limited voids thus increasing the material bulk density to 2.1 g/cm^3 and improving the compressive strength.

A clear trend emerges while evaluating the dimensional deviation ratio at different water-to-cement ratios, as shown in Fig. 7. This indicates that discrepancies between the actual printed and the intended dimensions increase at higher water-cement ratios. Mix I, which primarily consists of fine particles, shows a much larger dimensional deviation ratio across all axes concerning Mix II.

The xy-axis printing precision shown in Fig. 8 also confirms this trend. Each point is the average of three sets of four samples; error bars are also added to reflect variability. However, measurements involving layer shifting, clogging of the nozzle, or misinterpretation of CAD data were excluded. Notably, Mix-I is characterized by a higher discrepancy between the designed and the real dimensions than Mix-II, the effect being more evident for a larger water-to-cement ratio.

The findings of this study are consistent with earlier research [55], which showed that when the water-to-cement ratio increases, so does the flow rate, which in turn causes the fluid pressure to rise and stronger interlayer connections to form. However, our findings further explore the variables affecting the printing precision and dimensional deviation ratio in binder jetting. Mix-II, which contains coarser aggregate, has a strong structure that allows for efficient water absorption by the powder bed, limiting bleeding and promoting subsequent cement-particle contact. On the other hand, bleeding may deviate more from the 3D geometry dimension in Mix-I, which contains finer siliceous sand, resulting in enlarging the area where cement particles contact. In conclusion, our findings point out a decrease in printing accuracy as the water-to-cement ratio rises.

3. Conclusions

The present study investigated the effect of two different mixtures produced with coarse and fine siliceous sand and quick-setting cement at different w/c ratios on the mechanical properties and printing precision of BJ3DP components.

The following important conclusions can be drawn from this work:

- The significant difference in density between specimens with bigger and smaller aggregates points out the crucial impact of aggregate size; minor density changes were observed with increasing water-

cement ratio. The porosity of the specimen gradually decreases with increasing water/cement ratio.

- With the increase of the water-cement ratio flexural and compressive strength shows an increasing trend. The effect of different aggregate grain sizes, however, is negligible. Strength also improves significantly at longer curing time.
- Larger dimensional deviation ratios associated with finer aggregates highlight the need to adjust these parameters to achieve desired printing precision. In addition, decreasing the water-cement ratio improves printing accuracy.

In conclusion, Mix – II exhibits good mechanical properties as the water cement ratio increases. These findings suggest that the performance of 3D-printed concrete can be optimized by adjusting grain size distribution and water-to-cement ratio.

CRediT authorship contribution statement

Mursaleen Shahid: Writing – original draft, Visualization, Validation, Methodology, Investigation, Formal analysis, Data curation, Conceptualization. **Vincenzo M. Sglavo:** Writing – review & editing, Supervision, Resources, Project administration, Funding acquisition.

Declaration of competing interests

The authors declare that they have no known competing financial interests or personal relationships that could have appeared to influence the work reported in this paper.

Acknowledgments

We express our gratitude for the financial support provided by the Università di Trento.

References

[1] C. Gosselin, R. Duballet, P. Roux, N. Gaudillière, J. Dirrenberger, P. Morel, Large-scale 3D printing of ultra-high performance concrete – a new processing route for architects and builders, Mater. Des. 100 (2016) 102–109, https://doi.org/10.1016/J.MATDES.2016.03.097.

[2] I. Hager, A. Golonka, R.P.-P. Engineering, Undefined 2016, 3D Printing of Buildings and Building Components As the Future of Sustainable Construction?, Elsevier (n.d.). https://www.sciencedirect.com/science/article/pii/S1877705816317453 (accessed September 7, 2023).

[3] F. Bertolini, M. Mariani, E. Mercadelli, C. Baldisserri, C. Galassi, C. Capiani, R. Ardito, N. Lecis, 3D printing of potassium sodium niobate by binder jetting: printing parameters optimisation and correlation to final porosity, J. Mater. Res. Technol. 29 (2024) 4597–4606, https://doi.org/10.1016/J.JMRT.2024.02.145.

[4] X. Liu, X. Zhao, N. Wang, Y. Zhang, Z. Dai, Powder-based 3D printed magnesium phosphate cement: mechanical isotropy optimization using borax, Constr. Build. Mater. 432 (2024) 136660, https://doi.org/10.1016/J.CONBUILDMAT.2024.136660.

[5] O. Davtalab, A. Kazemian, B. Khoshnevis, Perspectives on a BIM-integrated software platform for robotic construction through Contour Crafting, Autom. Constr. 89 (2018) 13–23, https://doi.org/10.1016/J.AUTCON.2018.01.006.

[6] S.C. Paul, G.P.A.G. van Zijl, I. Gibson, A review of 3D concrete printing systems and materials properties: current status and future research prospects, Rapid. Prototyp. J. 24 (2018) 784–798, https://doi.org/10.1108/RPJ-09-2016-0154/FULL/HTML.

[7] F. Bos, R. Wolfs, Z. Ahmed, T.S.-V. and physical prototyping, undefined 2016, Additive manufacturing of concrete in construction: potentials and challenges of 3D concrete printing, Taylor Francis 11 (2016) 209–225, https://doi.org/10.1080/17452759.2016.1209867.

[8] M. Li, X. Wei, Z. Pei, C. Ma, Binder jetting additive manufacturing: observations of compaction-induced powder bed surface defects, Manuf. Lett. 28 (2021) 50–53, https://doi.org/10.1016/j.mfglet.2021.04.003.

[9] I. Gibson, D. Rosen, B. Stucker, M. Khorasani, Development of Additive Manufacturing Technology, Addit. Manufact. Technol. (2021) 23–51, https://doi.org/10.1007/978-3-030-56127-7_2.

[10] A. Mostafaei, A.M. Elliott, J.E. Barnes, F. Li, W. Tan, C.L. Cramer, P. Nandwana, M. Chmielus, Binder jet 3D printing—Process parameters, materials, properties, modeling, and challenges, Prog. Mater. Sci. 119 (2021) 100707, https://doi.org/10.1016/J.PMATSCI.2020.100707.

[11] F. Liravi, V. Jacob-John, A. Toyserkani, M. Vlasea, A Hybrid Method for Additive Manufacturing of Silicone Structures, (2017). https://doi.org/10.26153/16914.

[12] M. Shahid, V.M. Sglavo, Binder Jetting 3D Printing of Binary Cement—Siliceous Sand Mixture, Materials 17 (2024) 1514, https://doi.org/10.3390/MA17071514. Page 1514 17.

[13] M. Xia, B. Nematollahi, J. Sanjayan, Influence of Binder Saturation Level on Compressive Strength and Dimensional Accuracy of Powder-Based 3D Printed Geopolymer, Mater. Sci. Forum 939 (2018) 177–183, https://doi.org/10.4028/WWW.SCIENTIFIC.NET/MSF.939.177.

[14] M. Xia, B. Nematollahi, J. Sanjayan, Compressive strength and dimensional accuracy of portland cement mortar made using powder-based 3D printing for construction applications, RILEM Bookseries 19 (2019) 245–254, https://doi.org/10.1007/978-3-319-99519-9_23/FIGURES/5.

[15] M. Xia, B. Nematollahi, J. Sanjayan, Printability, accuracy and strength of geopolymer made using powder-based 3D printing for construction applications, Autom. Constr. 101 (2019) 179–189, https://doi.org/10.1016/j.autcon.2019.01.013.

[16] P. Shakor, S. Nejadi, G. Paul, Investigation into the effect of delays between printed layers on the mechanical strength of inkjet 3DP mortar, Manuf. Lett. 23 (2020) 19–22, https://doi.org/10.1016/j.mfglet.2019.11.004.

[17] P. Shakor, S. Nejadi, N. Gowripalan, Effect of Heat Curing and E6-Glass Fibre Reinforcement Addition on Powder-Based 3DP Cement Mortar, RILEM Bookseries 28 (2020) 508–515, https://doi.org/10.1007/978-3-030-49916-7_52/FIGURES/4.

[18] Z. Zhou, C. Mitchell, F. Buchanan, N. Dunne, Effects of Heat Treatment on the Mechanical and Degradation Properties of 3D-Printed Calcium-Sulphate-Based Scaffolds, ISRN Biomaterials 2013 (2012).

[19] B. Panda, S. Chandra Paul, M. Jen Tan, Anisotropic mechanical performance of 3D printed fiber reinforced sustainable construction material, Mater. Lett. 209 (2017) 146–149, https://doi.org/10.1016/J.MATLET.2017.07.123.

[20] P. Odaglia, V. Voney, B. Dillenburger, G. Habert, Advances in Binder-Jet 3D Printing of Non-cementitious Materials, RILEM Bookseries 28 (2020) 103–112, https://doi.org/10.1007/978-3-030-49916-7_11/FIGURES/7.

[21] New Trends in 3D Printing, (2016).

[22] G. Gibbons, R. Williams, P.P.-A. in A., Undefined 2010, 3D Printing of Cement Composites, 109, Taylor & Francis, 2010, pp. 287–290, https://doi.org/10.1179/174367509X12472364600878.

[23] E. Lloret, A.R. Shahab, M. Linus, R.J. Flatt, F. Gramazio, M. Kohler, S. Langenberg, Complex concrete structures: merging existing casting techniques with digital fabrication, Comput.-Aided Design 60 (2015) 40–49, https://doi.org/10.1016/J.CAD.2014.02.011.

[24] A.K. Maier, L. Dezmirean, J. Will, P. Greil, Three-dimensional printing of flash-setting calcium aluminate cement, J. Mater. Sci. 46 (2011) 2947–2954, https://doi.org/10.1007/S10853-010-5170-4/FIGURES/7.

[25] S. Benvenuti, F. Ceccanti, X. De Kestelier, Living on the Moon: topological Optimization of a 3D-Printed Lunar Shelter, Nexus. Netw. J. 15 (2013) 285–302, https://doi.org/10.1007/S00004-013-0155-7.

[26] M.K. Mohan, A.V. Rahul, G. De Schutter, K. Van Tittelboom, Early age hydration, rheology and pumping characteristics of CSA cement-based 3D printable concrete, Constr. Build. Mater. 275 (2021), https://doi.org/10.1016/J.CONBUILDMAT.2020.122136.

[27] A. Al Turk, G. Weheba, 3D printing of Portland cement using a binder jetting system, (2021). https://soar.wichita.edu/bitstream/handle/10057/24775/Turk/20and/20Weheba_v.14,no.1(2021).pdf?sequence=1 (accessed April 5, 2024).

[28] O. Na, K. Kim, H. Lee, H. Lee, Printability and Setting Time of CSA Cement with Na2SiO3 and Gypsum for Binder Jetting 3D Printing, Materials. (Basel) 14 (2021) 2811, https://doi.org/10.3390/MA14112811, 2021, VolPage 2811 14.

[29] P. Shakor, J. Sanjayan, A. Nazari, S. Nejadi, Modified 3D printed powder to cement-based material and mechanical properties of cement scaffold used in 3D printing, Constr. Build. Mater. 138 (2017) 398–409, https://doi.org/10.1016/j.conbuildmat.2017.02.037.

[30] P. Shakor, S. Nejadi, G. Paul, J. Sanjayan, A. Nazari, Mechanical Properties of Cement-Based Materials and Effect of Elevated Temperature on 3-D Printed Mortar Specimens in Inkjet 3-D Printing, ACI. Mater. J. 116 (2019) 55–67, https://doi.org/10.14359/51714452.

[31] A. Ur Rehman, V.M. Sglavo, 3D printing of Portland cement-containing bodies, Rapid. Prototyp. J. 28 (2022) 197–203, https://doi.org/10.1108/RPJ-08-2020-0195.

[32] J. Pegna, Exploratory investigation of solid freeform construction, Autom. Constr. 5 (1997) 427–437, https://doi.org/10.1016/S0926-5805(96)00166-5.

[33] D. Lowke, E. Dini, A. Perrot, D. Weger, C. Gehlen, B. Dillenburger, Particle-bed 3D printing in concrete construction – Possibilities and challenges, Cem. Concr. Res. 112 (2018) 50–65, https://doi.org/10.1016/j.cemconres.2018.05.018.

[34] A. Pierre, D. Weger, A. Perrot, D. Lowke, Penetration of cement pastes into sand packings during 3D printing: analytical and experimental study, Mater. Struct./Materiaux et Construct. 51 (2018) 1–12, https://doi.org/10.1617/S11527-018-1148-5/FIGURES/12.

[35] M. Xia, B. Nematollahi, J. Sanjayan, Compressive strength and dimensional accuracy of portland cement mortar made using powder-based 3D printing for construction applications, RILEM Bookseries 19 (2019) 245–254, https://doi.org/10.1007/978-3-319-99519-9_23/FIGURES/5.

[36] D. Lowke, D. Talke, I. Dressler, D. Weger, C. Gehlen, C. Ostertag, R. Rael, Particle bed 3D printing by selective cement activation – Applications, material and process technology, Cem. Concr. Res. 134 (2020), https://doi.org/10.1016/j.cemconres.2020.106077.

[37] P. McEleney, G. Walker, J. Orr, N.J. Dunne, Investigations on drop penetration and wetting characteristics of powder-liquid systems in relation to the mixing of acrylic

bone cement, Int. J. Nano Biomater. 3 (2010) 20–35, https://doi.org/10.1504/IJNBM.2010.036105.
[38] H. Miyanaji, N. Momenzadeh, L. Yang, Effect of printing speed on quality of printed parts in Binder Jetting Process, Addit. Manuf. 20 (2018) 1–10, https://doi.org/10.1016/J.ADDMA.2017.12.008.
[39] A. Butscher, M. Bohner, N. Doebelin, S. Hofmann, R. Müller, New depowdering-friendly designs for three-dimensional printing of calcium phosphate bone substitutes, Acta Biomater. 9 (2013) 9149–9158, https://doi.org/10.1016/J.ACTBIO.2013.07.019.
[40] P. Shakor, S. Nejadi, G. Paul, J. Sanjayan, Dimensional accuracy, flowability, wettability, and porosity in inkjet 3DP for gypsum and cement mortar materials, Autom. Constr. 110 (2020) 102964, https://doi.org/10.1016/j.autcon.2019.102964.
[41] D. Geldart, E.C. Abdullah, A. Hassanpour, L.C. Nwoke, I. Wouters, CHARACTERIZATION OF POWDER FLOWABILITY USING MEASUREMENT OF ANGLE OF REPOSE, CHINA PARTICUOL. 4 (2006) 3–4.
[42] M. Moghadasi, W. Du, M. Li, Z. Pei, C. Ma, Ceramic binder jetting additive manufacturing: effects of particle size on feedstock powder and final part properties, (2020). 10.1016/j.ceramint.2020.03.280.
[43] W. Du, X. Ren, Z. Pei, C. Ma, Ceramic Binder Jetting Additive Manufacturing: a Literature Review on Density, J. Manufact. Sci. Eng., Trans. ASME 142 (2020), https://doi.org/10.1115/1.4046248/1074276.
[44] Y.F. Ling, P. Zhang, J. Wang, Y. Shi, Effect of Sand Size on Mechanical Performance of Cement-Based Composite Containing PVA Fibers and Nano-SiO2, Mater. 13 (2020) 325, https://doi.org/10.3390/MA13020325. Page 325 13.
[45] J. Ingaglio, J. Fox, C.J. Naito, P. Bocchini, Material characteristics of binder jet 3D printed hydrated CSA cement with the addition of fine aggregates, Constr. Build. Mater. 206 (2019) 494–503, https://doi.org/10.1016/j.conbuildmat.2019.02.065.
[46] X. Fan, N. Travitzky, P. Greil, Y. Ma, X. Yin, X. Fan, N. Travitzky, P. Greil, Fabrication of MAX-phase-based ceramics by three-dimensional printing, Researchgate.Net (2015) 6–8, https://doi.org/10.4416/JCST2015-00006.
[47] S.Y. Chun, T. Kim, B. Ye, M.J. Lee, G. Lee, B. Jeong, H. Lee, H.D. Kim, Penetrated surface characteristics of cement - mixed sand in powder bed 3D printing, 10 (2022) 306–313. 10.1080/21870764.2021.2024734.
[48] P. Yang, S.K.A.O. Nair, N. Neithalath, Discrete element simulations of rheological response of cementitious binders as applied to 3D printing, RILEM Bookseries 19 (2019) 102–112, https://doi.org/10.1007/978-3-319-99519-9_10/FIGURES/7.
[49] L.N. Rabinskiy, S.A. Sitnikov, V.A. Pogodin, A.A. Ripetskiy, Y.O. Solyaev, Binder Jetting of Si3N4 Ceramics with Different Porosity, Solid State Phenomena 269 (2017) 37–50, https://doi.org/10.4028/WWW.SCIENTIFIC.NET/SSP.269.37.
[50] ASTM D7481, D7481 Standard Test Methods for Determining Loose and Tapped Bulk Densities of Powders using a Graduated Cylinder, (n.d.). https://www.astm.org/d7481-09.html (accessed September 7, 2023).
[51] EN 196-1:2016 - Methods of testing cement - Part 1: determination of strength, (n.d.). https://standards.iteh.ai/catalog/standards/cen/37b8816e-4085-4dcc-a642-a383d9bddd6c/en-196-1-2016 (accessed June 18, 2024).
[52] C642 Standard Test Method for Density, Absorption, and Voids in Hardened Concrete, (n.d.). https://www.astm.org/c0642-21.html (accessed November 6, 2024).
[53] T. Tracz, T. Zdeb, Effect of hydration and carbonation progress on the porosity and permeability of cement pastes, Materials. (Basel) (2019) 12, https://doi.org/10.3390/ma12010192.
[54] M. Abas, A. Salem, R.K. Pandey, Effect of Cement-Water Ratio on Compressive Strengthand Density of Concrete, n.d. www.ijert.org.
[55] F. Salari, P. Bosetti, V.M. Sglavo, Binder Jetting 3D Printing of Magnesium Oxychloride Cement-Based Materials: parametric Analysis of Manufacturing Factors, J. Manufact. Mater. Process. 2022 6 (2022) 86, https://doi.org/10.3390/JMMP6040086. Page 86 6.